Dielectronic Recombination Computations with the HULLAC Code

Ehud Behar

Department of Physics, Technion, Israel

Visiting Department of Astronomy, University of Maryland, USA

Outline

- The HULLAC Code
- Method: DW DR rates
- Results for W
- Laboratory Benchmarking
- Advanced Topics

HULLAC

- ***H****ebrew* ***U****niversity* ***L****awrence* ***L****ivermore* ***A****tomic* ***C****ode*
- Conceived by Marcel Klapisch, mostly written by Avi Bar-Shalom, with contributions by Joseph Oreg (Racah Algebra)
- Later programming contributions from Bill Goldstein, Michel Busquet and others
- New Collisional-Radiative version by M. Klapisch and M. Busquet

HULLAC Basic Approximations

- Parametric potential for energies
- Configuration mixing
- Distorted Wave
- Factorization Interpolation method for cross sections / rate coefficients
- Isolated resonance approximation, but DR+RR interference possible to compute

Relativistic Parametric Potential (PP) (Klapisch 1977)

- Treat e-e interactions as perturbation

$$H = H_0\left(\sum_{elec.i} h_i^{Dirac} + U^{PP}(\vec{r}_i)\right) + H_1\left(\sum_{elec.i} -Ze/r_i + e^2/r_{ij} - U^{PP}(\vec{r}_i)\right) + H_2(Breit + Lamb)$$

- PP $U(r_i)$ is a screened hydrogenic potential

$$U^{PP}(r) = -\frac{1}{r}\left[\sum_{shell\ s} q_s\, e^{-\alpha_s r}\, f_\ell(\alpha_s; r) + z\right] \qquad \sum_s q_s + z = Z$$

$$f_\ell(\alpha_s; r) = \sum_{j=0}^{2\ell+1}\left(1 - \frac{j}{2\ell+2}\right)\frac{(\alpha_s r)^j}{j!}$$

Level Energies

- PP is found through the variational principle by iterating α_s values to minimize level energies ΣE_l
- Used to produce complete set of single-electron orthogonal wavefunctions, and then asymmetric multi-electron states
- Perturbation theory with H_1 and H_2 yield final energies
- Clean, fast method that always converges and provides orthogonal wavefunctions suitable for bound and continuum rate coefficients

Factorization-Interpolation (Bar-Shalom et al. 1998)

$$\Omega_{ij}(\varepsilon) = 8 \sum_{j_i j_j J_T} \left| \left\langle \left(\psi_i, j_i(\varepsilon)\right) J_T \left| \sum_{k<l} \frac{1}{r_{kl}} \right| \left(\psi_j, j_j\right) J_T \right\rangle \right|^2$$

$\psi - bound\ state$

$j(nlj) - unbound\ elec$

- "Factorization" of electrostatic matrix element

$$\Omega_{ij}(\varepsilon) = 8 \sum_{j_i j_j J_T} \left\| \left\langle \psi_i \left| Z^T\left(j_i, j_j\right) \right| \psi_j \right\rangle \right\|^2 Q^T\left(j_i, j_j\right)$$

to "angular" and "radial" parts

Factorization-Interpolation (contd.)

- Separate bound electron coupling computed from Racah algebra
- Continuum/radial parts - both direct and exchange - integrals vary slowly with energy ε, which allows for efficient interpolation
- Extended to bound-free transitions, i.e., Autoionization (Oreg et al. 1991)

DR Method Recap

- Include all radiative and Auger channels
- Obtain E_{di}, A, and A^a rates from code
- Test for and include configuration mixing
- For rate coefficients
  - Convolve with Maxwellian (T_e)
  - Add up thousands of doubly excited level contributions
  - Extrapolate to high-n high-l (plasma dependent)
  - Fit with few-component exponential function (optional)
- For beam experiments
  - Compute resonance strength
  - Convolve with beam profile
  - Identify resonances

DR Coefficients - Capture

- Cross Section and Resonance Strength
  (*i* – initial, *d* – doubly excited, electron $\varepsilon = E_d - E_i = E_{di}$)
  - Narrow natural-width Lorentizan profile $L_d(\varepsilon)$

$$\sigma_{id}^{DC}(\varepsilon) = \frac{g_d}{2g_i}\frac{(2\pi\hbar)^3}{8\pi m\varepsilon}A_{di}^a L_d(\varepsilon)$$

$$S_{id}^{DC} = \int \sigma_{id}^{DC}(\varepsilon)d\varepsilon = \frac{g_d}{2g_i}\frac{(2\pi\hbar)^3}{8\pi m(E_d - E_i)}A_{di}^a$$

- Capture Rate Coefficient

$$\beta_{id}^{DC}(T_e) = <\sigma v>_{Maxwell} = \frac{g_d}{2g_i}\left(\frac{2\pi\hbar^2}{mkT_e}\right)^{3/2} A_{di}^a e^{-E_{di}/kT_e}$$

DR Coefficients - Stabilization

- Branching ratio for stabilization

$$B^D(d) = \frac{\sum_{j<d} A_{dj} + \sum_{i<d'<d} A_{dd'} B^D(d') + \sum_{d''<i<d} A_{dd''}}{\sum_{i'} A^a_{di'} + \sum_{j<d} A_{dj} + \sum_{i<d'<d} A_{dd'} + \sum_{d''<i<d} A_{dd''}}$$

- With low lying doubly excited levels, decays to unbound (d') and stabilization to bound (d'') doubly excited levels can be important
- Decays to unbound levels can be followed by autoionization or by further decay

Non-Resonant Decays

TABLE III. Ratios of the rate coefficients for DR through the $3d^9 4ln'l'$ ($n'=4,5$) complexes calculated including NRS and DAC processes to coefficients obtained by taking into account resonant transitions only. For each ion the first line displays the results including NRS and the second line the total results including NRS and DAC.

Ion		T_e 10 eV	20 eV	100 eV	1000 eV	10 000 eV
		$3d^9 4l4l'$ complex				
Mo^{14+}	NRS	2.48	1.78	1.16	1.08	1.08
	NRS+DAC	2.50	1.86	1.30	1.19	1.19
Pr^{31+}	NRS	1.47	1.25	1.08	1.03	1.03
	NRS+DAC	1.47	1.25	1.09	1.05	1.05
Gd^{36+}	NRS	1.36	1.15	1.06	1.03	1.03
	NRS+DAC	1.36	1.15	1.07	1.04	1.04
Ta^{45+}	NRS	1.75	1.30	1.07	1.03	1.03
	NRS+DAC	1.75	1.30	1.07	1.04	1.03
U^{64+}	NRS	1.04	1.03	1.02	1.02	1.02
	NRS+DAC	1.04	1.02	1.02	1.02	1.02
		$3d^9 4l5l'$ complex				
Mo^{14+}	NRS	10.82	3.32	1.26	1.15	1.14
	NRS+DAC	10.94	3.61	1.45	1.25	1.24
Pr^{31+}	NRS	18.86	5.11	1.76	1.13	1.11
	NRS+DAC	18.86	5.11	1.85	1.20	1.16
Gd^{36+}	NRS	32.45	6.72	2.01	1.21	1.17
	NRS+DAC	32.45	6.72	2.01	1.23	1.20
Ta^{45+}	NRS	45.58	16.11	2.13	1.21	1.17
	NRS+DAC	45.58	16.11	2.14	1.24	1.19
U^{64+}	NRS	69.30	4.46	1.44	1.26	1.21
	NRS+DAC	69.30	4.46	1.44	1.25	1.19

Low Lying Resonances

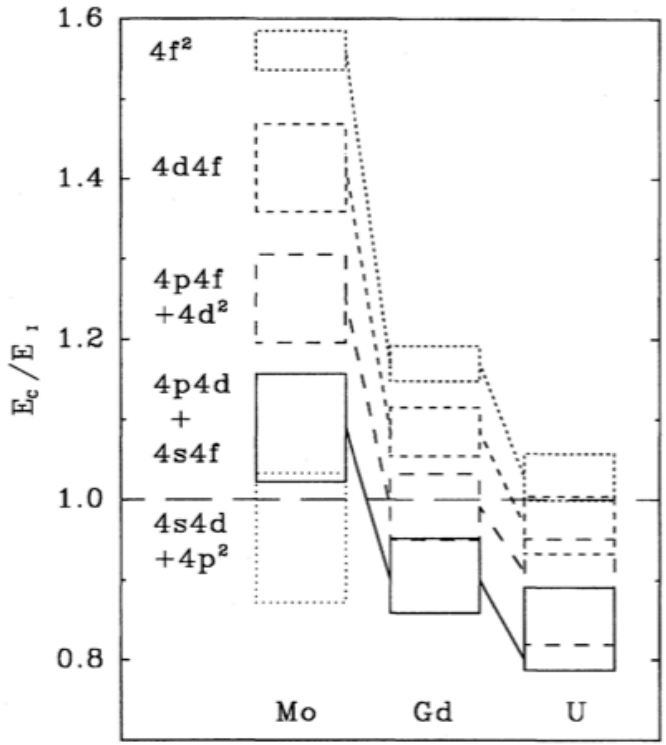

FIG. 1. Energy E_c of the inner-shell excited configurations within the $3d^9 4l4l'$ complex relative to the first ionization limit E_I for three elements in the Cu I isoelectronic sequence. For the Gd^{35+} and U^{63+} Cu-like ions the $3d^9[4s4d+4p^2]$ mixed configurations are well below the ionization limit, and are not plotted. The energies are indicated by a finite vertical range representing the full level spread within each configuration.

Low Resonances – All the Trouble

$$\beta_{id}^{DC}\left(T_e\right) \propto e^{-E_{di}/kT_e}$$

- Sensitive to code accuracy
- Resonance yields maximum contribution at $kT_e = 2/3\ E_{di}$
- Low/high resonances contribute at low/high temperatures

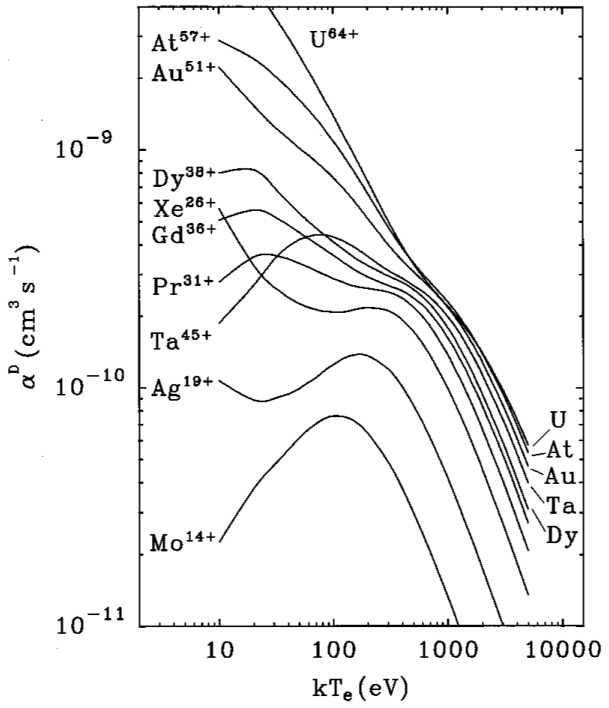

FIG. 4. Total DR rate coefficients for the ten Ni-like ions considered, as a function of the electron temperature.

Not for Fusion Plasmas, but

- Photoionized plasmas tend to be highly-ionized but cold $kT_e << E_{Ion}$
- DR resonances of the lowest lying doubly excited levels are dominant

Savin et al. 2002

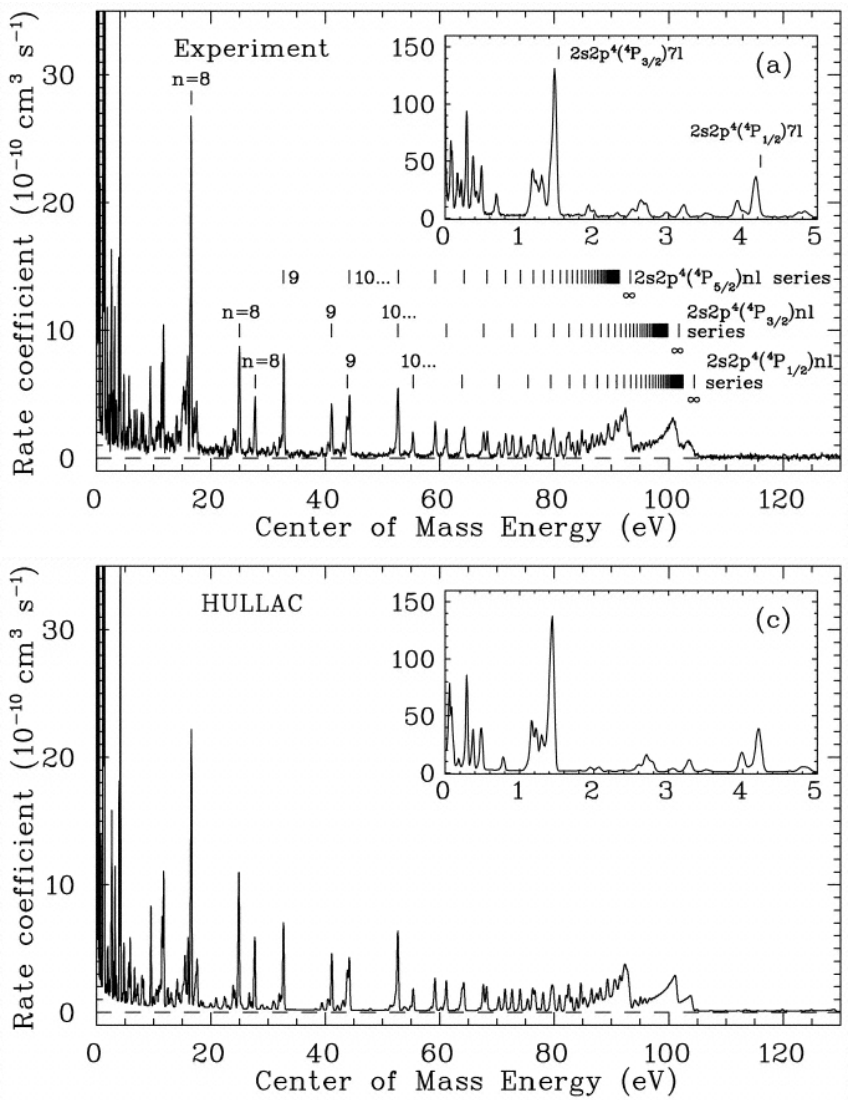

Savin et al. 2002 (contd.)
Resonance Strengths & Rate Coefficients

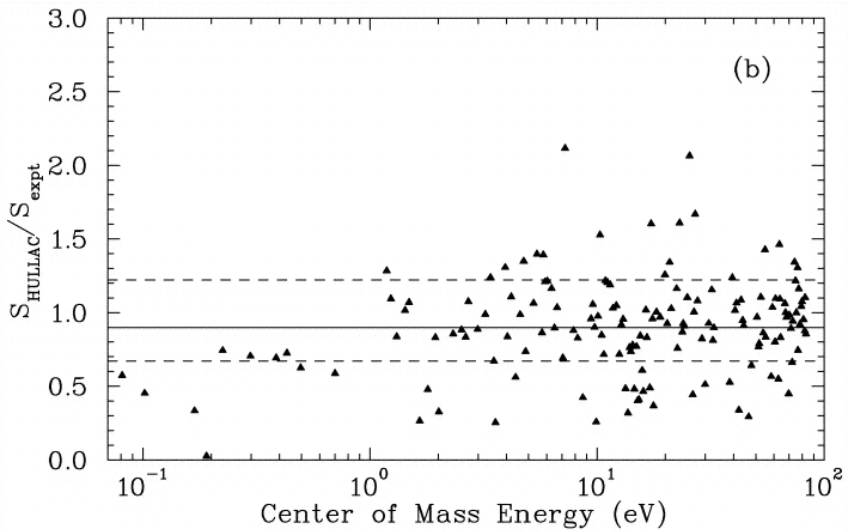

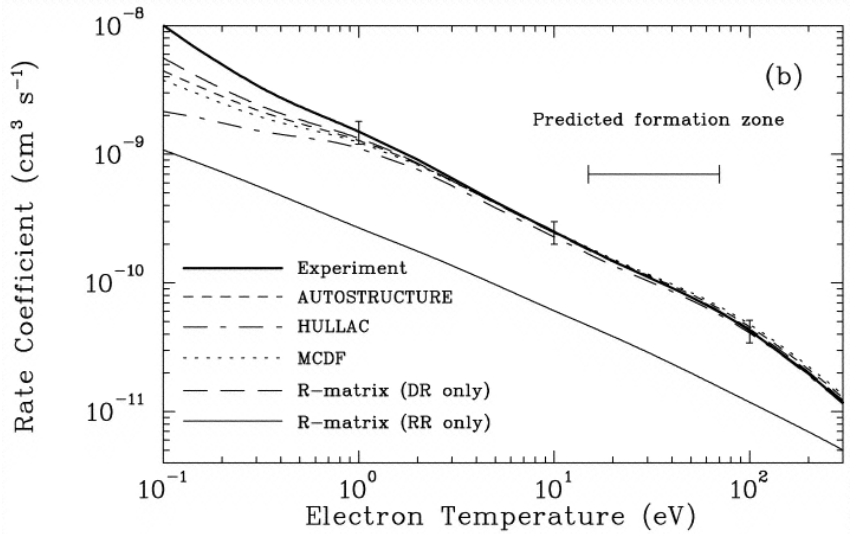

For high-lying levels n^{-3} Scaling

$$\alpha_{idf}^{D}(T_e) = \beta_{id}^{DC}(T_e) B^{D}(d) \propto \frac{A_{di}^{a} A_{df}}{A_{di}^{a} + A_{df}}$$

$$\psi^{bound} \propto n^{-3/2}$$

$$\Rightarrow for \Delta n > 0 \; A_{di}^{a}, A_{df} \propto n^{-3}$$

$$\Rightarrow \alpha_{id}^{DC}(T_e) \propto n^{-3}$$

$$for \Delta n = 0 \; A_{df} \propto n^{0}$$

and mixed cases

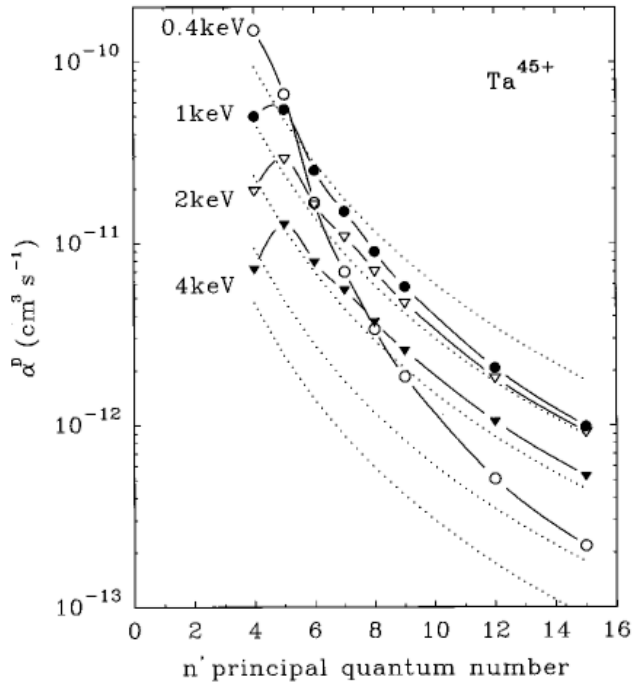

FIG. 3. Partial rate coefficients for DR of Ta^{45+} through the various $3d^9 4ln'l'$ configuration complexes as a function of the principal quantum number n' in the $n'=4$–15 range, for four selected temperatures. The solid curves are plotted through the calculated values just to guide the eye. The dotted curves indicate the n'^{-3} grid as reference for the scaling of the partial rate coefficients.

What About High-*l* ?

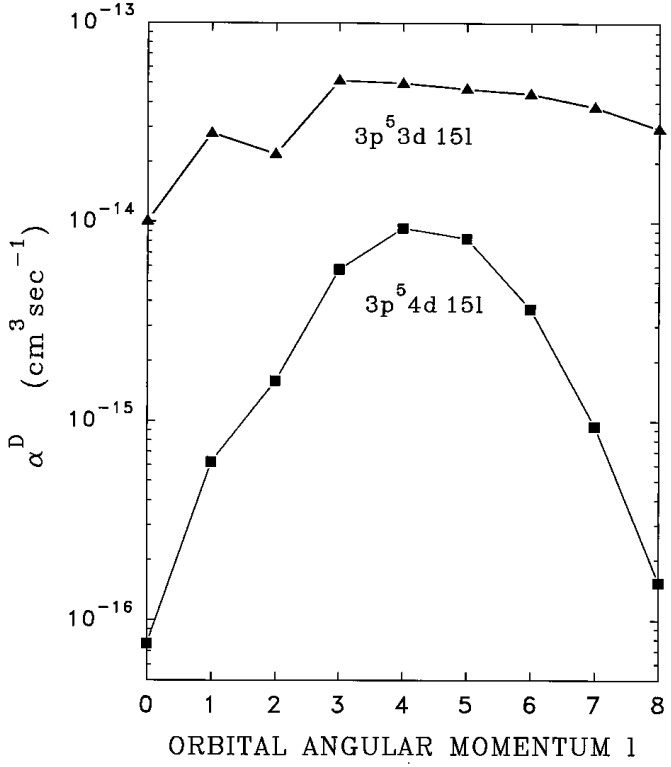

FIG. 1. Partial rate coefficients for DR through the configurations $3p^5 3d 15l$ (triangles) and $3p^5 4d 15l$ (squares) as a function of the orbital angular momentum quantum number l, at an electron temperature of 7 keV. The lines between the calculated values are plotted just to guide the eye.

High-*n* and Low-*E*

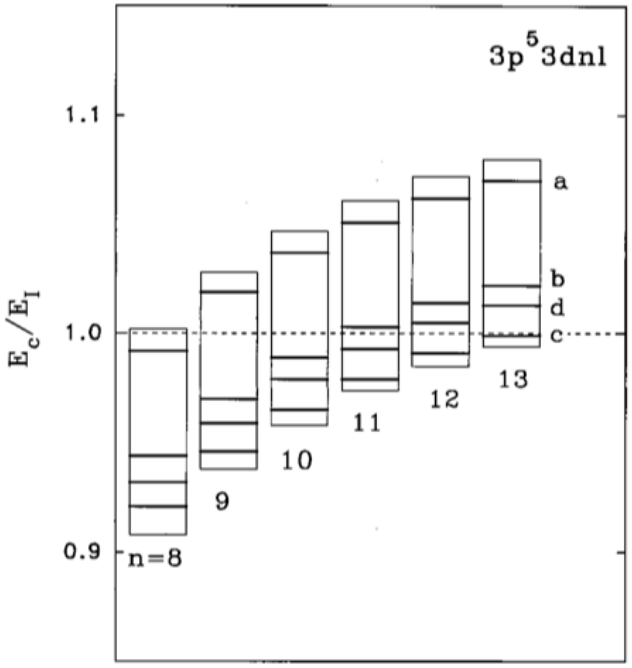

FIG. 6. Energy E_c of the inner-shell excited configuration complexes $3p^5 3dnl$ $8 \leqslant n \leqslant 13$ relative to the first ionization limit E_I. The energies are indicated by a finite vertical range representing the full level spread within each complex. The four thick lines in each complex stand for the mean energy of the four dominant groups of levels (regarding their contributions to the DR rate coefficient). The alphabetic order of the groups is according to the significance of their contributions.

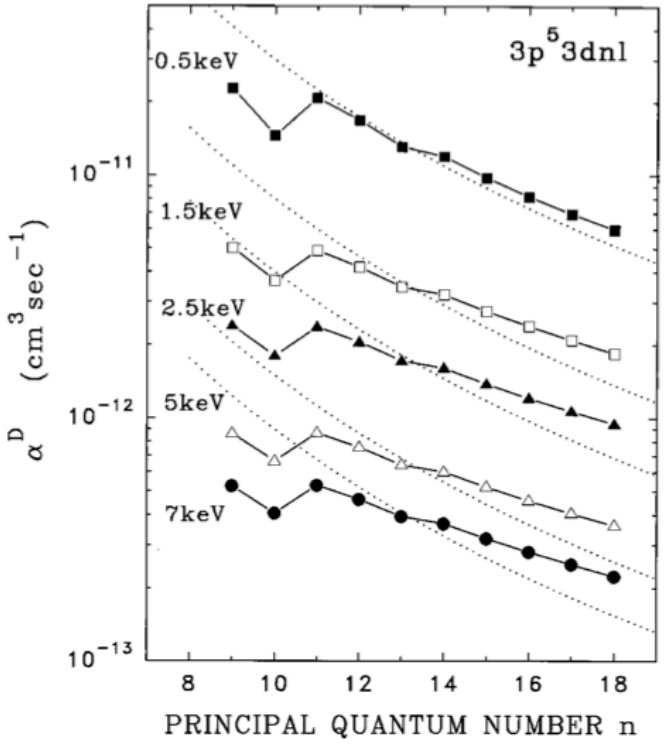

FIG. 7. DR rate coefficients through the complexes $3p^5 3dnl$ as a function of the principal quantum number n in the range $9 \leqslant n \leqslant 18$ at five different electron temperatures. The solid lines between the calculated values are plotted just to guide the eye. The dotted curves indicate the n^{-3} grid as a reference for the scaling of the rate coefficients.

Ar-like W

Benchmarking Computed DR Data with the Electron Beam Ion Trap

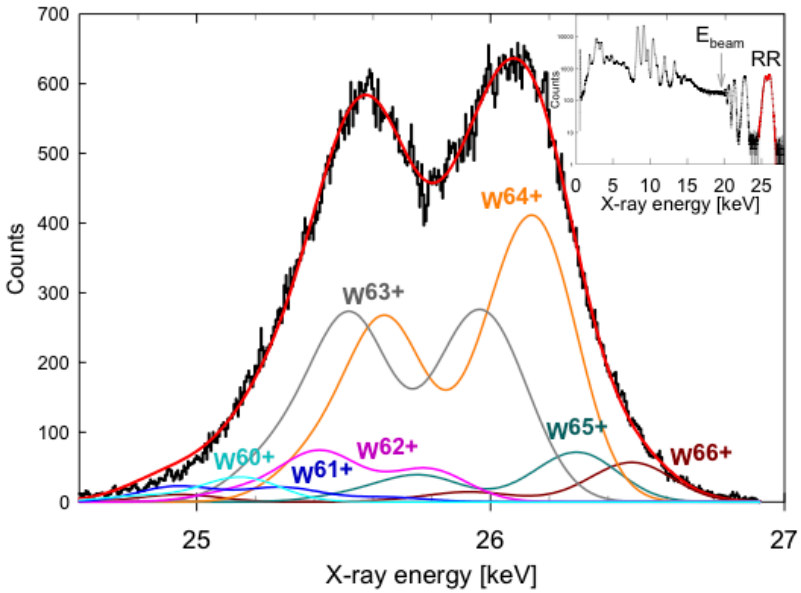

Figure 1: X-ray spectrum showing the detail of n=3 radiative recombination of highly charged tungsten ions. The black quivering line marks the observed intensity and is fitted by the ***nl*** contribution of W^{60+} to W^{67+} ions (colored lines) which sum up to the red line and gives the charge state distribution. The inset presents the wide range spectrum produced in EBIT at 20 keV electron beam energy with a logarithmic intensity scale. The spectrum is dominated by n=2-3 direct excitation lines between 8 and 13 keV rising above the Bremsstrahlung background.

N-like to Si-like W
Biedermann et al. 2009

Benchmarking Computed DR Data (contd.)

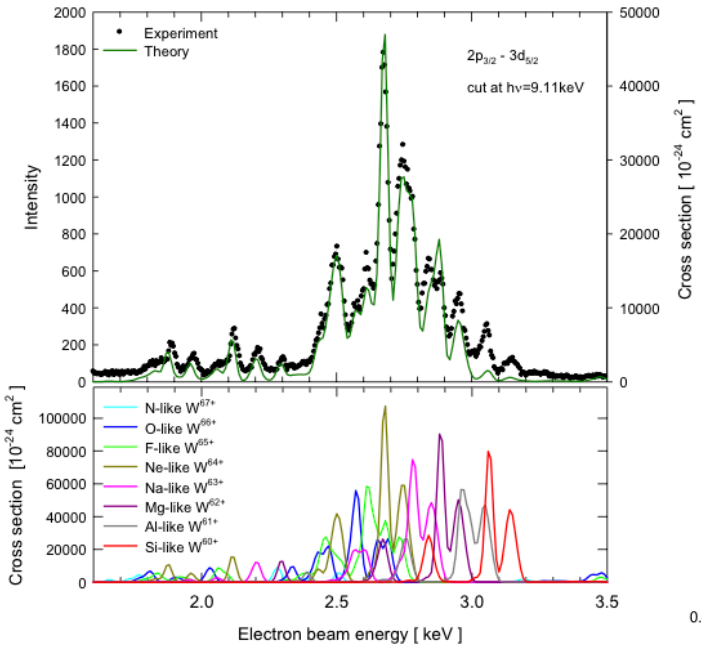

Figure 2. Comparison of measured and calculated LMM dielectronic recombination resonance cross section of highly charged tungsten ions (q=60+ to 67+). Shown here is the part of the LMM DR process during which a $2p_{3/2}$-electron is excited to $3l$, while a free electron recombines to $3l'$. The doubly excited state relaxes by emission of an x-ray following a $2p_{3/2}$ - $3d_{5/2}$ transition.

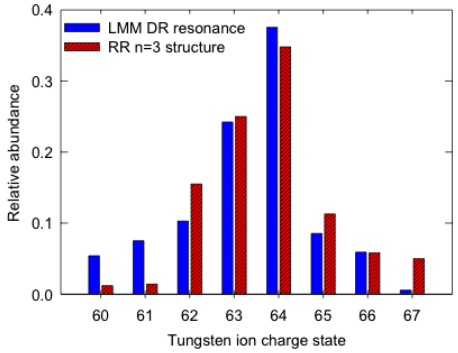

Figure 3: Charge state abundance of tungsten ions determined from the measured radiative recombination intensity at 20 keV, 100 ms before the DR ramp (red, hatched) and from a fit of the theoretical resonance strength to the observed LMM DR intensity.

Biedermann et al. 2009
LMM (LMN) resonances

Advanced Topics

based on elegant methods by V. Jacobs

- Plasma density effects

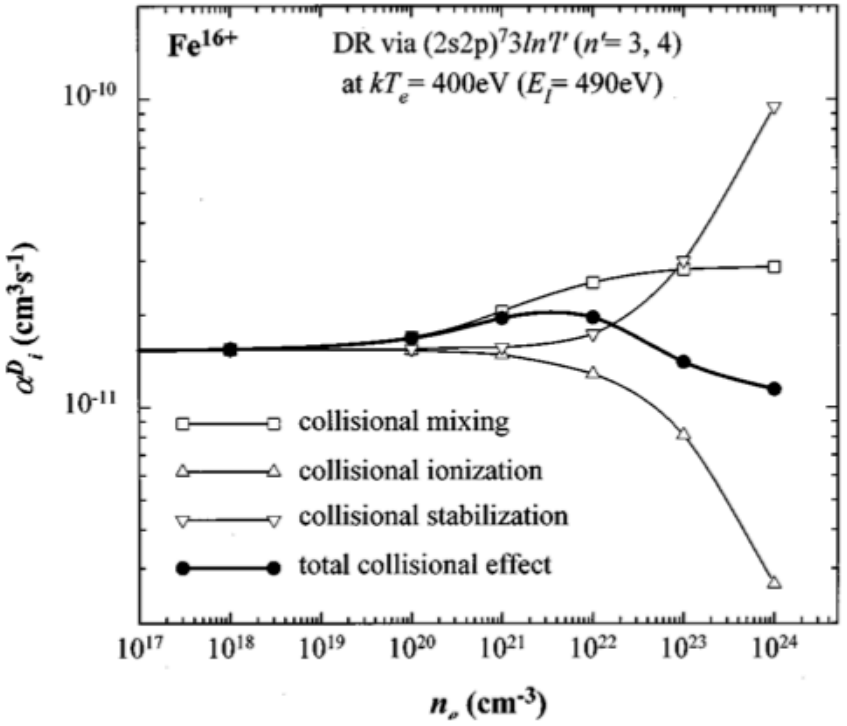

- RR + DR interference (Fano profile cross-sections)

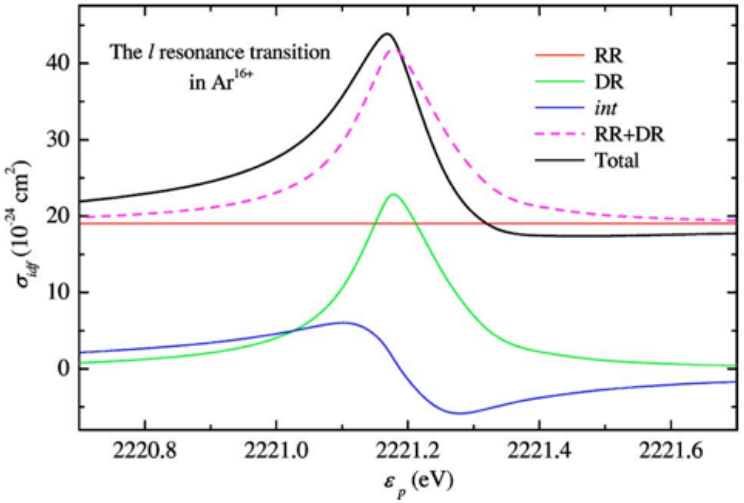

- Not dramatic for rates
- C.f. R-matric methods

Summary & Questions

- DR calculations are challenging and difficult to mass-produce
- Need to carefully inspect several effects on a case by case basis
  - High - *n*
  - High - *l*
  - Non-resonance stabilization
  - Decays to autoionizing levels
  - Density effects
- Refinements can be tedious
  - need to define the accuracy required
- Benchmarking with experiments is invaluable